Cogn Neurodyn (2010) 4:133–149
DOI 10.1007/s11571-010-9107-z

ORIGINAL RESEARCH

# A method for the estimation of functional brain connectivity from time-series data

**A. Wilmer · M. H. E. de Lussanet · M. Lappe**

Received: 16 April 2009 / Revised: 5 February 2010 / Accepted: 11 February 2010 / Published online: 6 March 2010


**Abstract** A central issue in cognitive neuroscience is which cortical areas are involved in managing information processing in a cognitive task and to understand their temporal interactions. Since the transfer of information in the form of electrical activity from one cortical region will in turn evoke electrical activity in other regions, the analysis of temporal synchronization provides a tool to understand neuronal information processing between cortical regions. We adopt a method for revealing time-dependent functional connectivity. We apply statistical analyses of phases to recover the information flow and the functional connectivity between cortical regions for high temporal resolution data. We further develop an evaluation method for these techniques based on two kinds of model networks. These networks consist of coupled Rössler attractors or of coupled stochastic Ornstein–Uhlenbeck systems. The implemented time-dependent coupling includes uni- and bi-directional connectivities as well as time delayed feedback. The synchronization dynamics of these networks are analyzed using the mean phase coherence, based on averaging over phase-differences, and the general synchronization index. The latter is based on the Shannon entropy. The combination of these with a parametric time delay forms the basis of a connectivity pattern, which includes the temporal and time lagged dynamics of the synchronization between two sources. We model and discuss potential artifacts. We find that the general phase measures are remarkably stable. They produce highly comparable results for stochastic and periodic systems. Moreover, the methods proves useful for identifying brief periods of phase coupling and delays. Therefore, we propose that the method is useful as a basis for generating potential functional connective models.

**Keywords** Functional connectivity · Time-delayed phase synchronization · MEG magnetencephalography · Network analysis

A. Wilmer (✉) · M. H. E. de Lussanet · M. Lappe
Deptartment of Psychology, Westf. Wilhelms-University, Otto Creutzfeldt Center for Cognitive and Behavioral Neuroscience (OCC), Münster, Germany
e-mail: andreas.wilmer@uni-muenster.de

## Introduction

Exploring the flow of information in the brain is a central issue in cognitive neuroscience. Although the development of imaging techniques (Toga and Mazziotta 2002) has provided strong tools for measuring functional and local changes of brain activity, such techniques are not optimal for measuring the flow of information across the brain.

Investigating the dynamics of cognitive processes in the brain demands a high temporal resolution. This can be achieved by imaging via EEG or MEG (Pfurtscheller and da Silva 1999). In addition to having a higher time resolution than the alternative techniques fMRI and PET, MEG and EEG have the advantage that they detect primary neuronal activities, whereas fMRI and PET measures metabolic correlates. The disadvantage of EEG and MEG as compared to metabolic techniques is that they have a lower resolution, more smear, and—especially EEG—more distortion as a result of inhomogeneous conductive properties of the tissues. In practice the spatial resolution of MEG is limited to about 5 mm (Barnes et al. 2004; Murakami et al. 2002). Such reconstructed MEG source activities might be the starting point for dedicated analyses of functional connectivity as verified by Hadjipapas et al. (2005). Ideally, a method for estimating functional connectivity should take into account the non-stationary state of the brain during a cognitive task. Thus, a trial-based

statistical approach is preferable. Such localized functional time series of neuronal activity can be gained from MEG data by beamforming techniques (Gross et al. 2001; Herdman et al. 2003; Robinson and Vrba 1998; Van Veen et al. 1997) as well as other methods such as minimum norm (Hämäläinen and Ilmoniemi 1994).

The aim of the present work is to develop a tool for estimating functional connectivity by computing phase synchronization between time series. We apply known bivariate data-driven analysis techniques and expand them in such a way that we can construct patterns of connectivity, which comprehend arbitrary temporal and arbitrary delayed interactions. The goal is to make as little a priori assumptions as possible. First, we do not enter information about the direction of connectivity of the sources. Second, the connectivity may be non-stationary. Third, the connectivity may be delayed by an unknown amount. Fourth, the synchronization measure is based on relative phases, and is therefore independent of signal amplitude. We do further investigations on those connectivity patterns by a quantification of different measures and the application of a statistical rating.

We will generate synthetic data using two complementary models containing brief, delayed periods of synchronization. Since the amount of synchronization between measured MEG signals is not known, we use synthetically generated data for developing and testing our methods with an exactly defined connection structure. With those, synthetic data networks of various delays, coupling strengths, and driving directions can be generated.

Each estimate of synchronization critically depends on definition of phase and relative phases. This is a nontrivial problem for non-stationary systems. Synchronization is a universal phenomenon appearing in nonlinear systems. However, there exists no unique interpretation for the notion of synchronization. A generalized description of synchronization exists in the field of nonlinear dynamics, and in the exploration of chaotic systems (Rulkov et al. 1995). Consider a dynamical system such as a Rössler oscillator (cf. section "Coupled Rössler oscillator", Eq. 17), which evolutes on an attractor in a 3-dim phase space. Coupling two such systems results in a solution, that is embedded in a 6-dim solution space. If the two systems are synchronized (as a result of the coupling) their phase spaces will be more similar. This can be understood as the collapsing of the total evolution onto a subspace, which is generally valid for any number of synchronous systems (Rulkov et al. 1995). A simplistic and naive approach to synchronization would be to threshold the coincidence of the states of interacting individual systems. A more general and sophisticated way to describe synchronization was developed by Pikovsky et al. (2003). In their approach the phase of a signal is defined with the help of the analytic signal concept (Gabor 1946), which can be estimated even for chaotic or noisy time series. This definition plays a central role in detecting synchronization. Pikovsky et al. found different regimes of synchronization: from non-synchronous to phase synchronous, to a lag synchronization and into a complete synchronized state with a decreasing coupling strength (Brown and Kocarew 2000; Rosenblum et al. 1997).

The phase synchronization of two complex systems can be defined as the appearance of a certain entrainment of the phase difference of the interacting systems. This allows the introduction of a quantitative measure (Rosenblum et al. 2001, 1996). The amplitudes might remain uncorrelated. A detailed discussion of the notion of phase can be found in Pikovsky et al. (2003) and Boccaletti et al. (2002).

In section "Methods" we develop a bivariate analysis technique for estimating directional, time-dependent coupling within a network of neuronal signals. A moving time average technique is proposed for the application on small data-sets (in the range of 100–150 trials), which are common in experimental settings. Furthermore, we introduce the Jensen–Shannon divergence, in order to have an objective and quantitative measure for comparing the simulations.

In section "Results" we apply two artificial networks for studying and evaluating the analysis techniques of section "Methods": in section "Aperiodically driven stochastic processes" an Ornstein–Uhlenbeck process—a special form of a stochastic first-order dynamical system—is proposed for the generation of fluctuating time series. The system consists of two identically coupled noise driven subsystems. The stochastic receiver is exposed to a stochastic driver, which results in a synchronization to the driving system.

In section "Coupled Rössler oscillator" we present as a second example a coupled system of two nonidentical Rössler oscillators. Neuronal dynamics cover the spectrum from nonlinear chaotic behavior on a microscopic level to nearly oscillatory stochastic dynamics on a macroscopic level (Atmanspacher and Rotter 2008; Pereda et al. 2005). Coupled Rössler systems are commonly used to generate complex oscillatory data, because they provide a good control over the synchronization between pairs of such oscillators (Rosenblum et al. 1996; Schelter et al. 2006). By virtue of this property, Rössler systems are often implemented to test the properties of new tools for neuronal synchronization (Hadjipapas et al. 2005; Quian Quiroga et al. 2002; Quyen et al. 1998). We model the interactions within a network of Rössler oscillators among each other with a linear coupling lasting for small windows in time and delay for every oscillator couple.

In both, the Ornstein–Uhlenbeck and the Rössler system, the subsystems are interconnected in such a dynamic time delayed fashion: to model feedback and feedforward loops the two dimensional coupling term depends on time

and on the time lag between the driving and the receiving system. The proposed models for generating the synthetic data are not supposed to simulate the dynamic of electrophysiological data as EEG or MEG directly. They represent two complementary, a stochastic and an oscillatory one, in order to capture two aspects of natural neuronal behavior.

On the basis of this synthetic data some interesting effects in the connectivity patterns are discussed in section "Artifacts in bivariate network analysis" for a 3 × 3 network. A quantitative view on the connectivity patterns is done by defining a significance threshold.

## Methods

### Estimation of the phase

The first step in exploring the phase synchronization between two time series requires the estimation of the phase differences. In the case of a harmonic signal the phase is directly proportional to the time, but for arbitrary fluctuating signals a general concept of phase has to be proposed. Such a concept has been developed in nonlinear physics and chaos theory and was explored in detail (Rosenblum et al. 1996). The estimation of the phase can be managed by an embedding of a real time series $s(t)$ in the two-dimensional complex plane $(s, \mathcal{H}_t\{s(t)\})$ (Gabor 1946). The resulting complex time series $z(t)$ forms the analytic complex signal generated by the Hilbert transformation $\mathcal{H}_t\{.\}$ :

$$z(t) = s(t) + i\mathcal{H}_t\{s(t)\} = A(t)\, e^{i\phi(t)} \tag{1}$$

where $A(t)$, the instantaneous amplitude, and $\phi(t)$, the instantaneous phase, are unambiguous. The integral transformation $\mathcal{H}_t\{.\}$ can be calculated considering the Cauchy principal value (P.V.):

$$\mathcal{H}_t\{s(t)\} = \frac{1}{\pi}\mathrm{P.V.}\int_{-\infty}^{\infty} \mathrm{d}t' \frac{s(t')}{t - t'} \tag{2}$$

A crucial property of the Hilbert transformation is that it conserves the spectrum of the signal, so that the dynamics of frequency and phase remain unbiased. Equation (2) can be implemented numerically by using the discrete Fourier transformation. The filter operation is done with an amplitude response of one, a phase shift of the signal with $-\frac{\pi}{2}$ for all positive and a shift of $\frac{\pi}{2}$ for all negative frequency components in the complex Fourier space. We deliberately chose the Hilbert transformation, and not to embed the time series with the time derivative $(s, \dot{s})$ as in classical mechanics, and neither to apply an embedding based on a time lag $(s, s(t - \tau))$. The disadvantage of these methods as compared to the embedding with the Hilbert transformation is that these result in an artificial jittering of the phase due to a wrong scaling of the embedding dimension.

Next, the phase can be calculated easily from Eq. (1) using the imaginary and real part of $z(t)$:

$$\phi(t) = \arctan\left(\frac{Im\{z(t)\}}{Re\{z(t)\}}\right) \tag{3}$$

We eliminate DC-offsets by subtracting the average over the time before calculating the analytic signal to ensure that the centre of the oscillation is in the origin of the coordinate system.

### Detecting phase synchronization

Equipped with this knowledge we can now explore phase synchronization. In this section we illustrate the general concept of two index-based measures of phase synchronization. The first, $\gamma_{nm}$, is usually called *phase coherence* or *phase locked value* (PLV) and is an average-based measure (Hoke et al. 1989; Lachaux et al. 1999; Mormann et al. 2000; Rosenblum et al. 1997; Stam et al. 2007; Varela et al. 2001). The second synchronization index, $\rho_{nm}$, is based on the Shannon entropy (Tass et al. 1998).

Let the phase of two oscillating systems be dependent on the systems themselves and on the coupling mechanism. Then the amplitudes may be uncorrelated, even if the two systems are in a synchronized state. Importantly, weak interactions can be revealed in cases in which techniques dealing not with phase measures, like amplitude based techniques, may fail. Consider two stochastic time series $S_k^{(j)}(t)$ and $S_l^{(j)}(t)$, which each may represent the reconstructed neuronal activities at locations '$k$' and '$l$' in the source space, over a set of trials $j = 1, \ldots, N$. The time $t \in [0, T]$ is limited by the trial length $T$. After the calculation of the phase with Eq. (3) a pairwise estimation of the general phase difference can be performed.

$$\Delta\Phi_{nm}(t;\tau) = n\Phi_k(t) - m\Phi_l(t - \tau) \tag{4}$$

We here introduce the variable $\tau$, which specifies the parametric time delay for the construction of a connectivity pattern. It is limited to the interval $\tau \in [0, t)$. Equation (4) cannot be estimated if the delay parameter $\tau$ is longer than the current time value $t$ due to missing overlap of the shifted data. By shifting the time the direction of driving can be identified, i.e. the process can be separated into a driving system at an earlier time $t - \tau$ and a responding or driven system '$k$' at time $t$. Notice that $\tau \geq 0$ by definition because a negative $\tau$ implies that system '$k$' drives '$l$' with a positive $\tau$. The indices $n, m \in \mathbb{N}^+$ specify the order of synchronization and can be chosen arbitrarily. If we assume linear coupling, the ratio of the indices can be chosen $n$:$m$ = 1:1. In general a $n$:$m$ synchronization denotes how the frequencies interact,

e.g. in a synchronized $n = 2, m = 1$ the driver '$l$' oscillates with the double frequency as the responder '$k$'. The description of phase synchronization in noisy systems requires the boundedness of $\Delta\Phi_{nm}(t;\tau)$ as a phase locking condition, i.e. the phase difference remains finite in the limit of large times:

$$|\Delta\Phi_{nm}(t;\tau)| < const$$

This condition is meant for unwrapped phases $\phi \in \mathbb{R}$. Strictly one has to consider phase jumps due to the $2\pi$ periodicity of the tan function (Eq. 3), by tracing the phase position in the complex plane. If the phase switches the quadrant in the complex plane, offsets in the phase time series have to be included. For noisy data a correct unfolding of the phase is an arduous task due to noise-induced phase-slips in both directions. As we will see below, one can simply use the periodic phases to measure the phase synchronicity, so that the step of unwrapping the phase can be skipped.

The phase-locked value (PLV), $\gamma_{nm}$, is an average-based measure. Let $j = 1, \ldots, N$ denote the index for the trials and $\langle S^{(j)}(t)\rangle$ the average over a moving time window of $\Delta T$ for a set $\{S^{(1)}(t), \ldots, S^{(N)}(t)\}$ of an arbitrary stochastic time-series with $N$ realizations:

$$\langle S^{(j)}(t)\rangle = \frac{1}{\Delta T}\int_{t-\frac{\Delta T}{2}}^{t+\frac{\Delta T}{2}} \mathrm{d}t' \frac{1}{N}\sum_{j=1}^{N} S^{(j)}(t') \tag{5}$$

The moving average technique results in a smoother solution. The window size $\Delta T$ gives a lower limit for recovering periods of synchronization. In other words, there is a trade-off between temporal resolution and signal to noise ratio. We thus obtain the following expression for the phase coherence as in (Mormann et al. 2000) considering an additional parametric delay:

$$\gamma_{nm}(t;\tau) = |\langle e^{i\Delta\Phi_{nm}^{(j)}(t;\tau)}\rangle| \tag{6}$$

This equation can be understood as the summation of position vectors on the unit circle in the complex plane. The orientation of each vector is given by its phase difference $\Delta\Phi_{nm}(t)$ and their mean value is formed over all trials $j$ within a certain time window $\Delta T$. The resulting averaged length is given by its absolute value and is a degree of synchronization. For two non-synchronous processes these vectors will be uniformly distributed and will sum up to zero. In a synchronized state, the phase difference vectors are not uniformly distributed, so that a statistically preferred direction for all vectors exists (Fig. 1a). Completely synchronized processes are indicated by $\gamma_{nm} = 1$. Repeating this procedure for all data points $0 < t < T$ and all delay parameter $0 \leq \tau < t$ leads to a pattern of synchronization $\gamma_{nm}(t;\tau)$.

The second synchronization index, $\rho_{nm}$, is based on the Shannon entropy. This measure requires that a phase is defined on a periodic interval. The cyclic relative phase in the interval $[-\pi, \pi]$ is given by:

$$\Psi_{nm}(t;\tau) = (\Delta\Phi_{nm}(t;\tau) + \pi)\mathrm{mod}2\pi - \pi \tag{7}$$

Next, a periodic probability density function (PDF) over all trials and a time window $\Delta T$ can be calculated from Eq. (7) cf. Risken and Frank (1996) with

$$p_{nm}(\psi, t;\tau) = \langle\delta(\psi - \Psi_{nm}^{(j)}(t;\tau))\rangle \tag{8}$$

where $\delta(.)$ denotes the Dirac delta function. For a numerical estimation of the PDF we use an adaptive discretization of the cyclic variable $\psi$ following the suggestions by Otnes and Enochson (1972). An estimator of the total bin number is given for $T$ data points by:

$$\mathrm{BIN} = \exp(0.626 + 0.4\ln(T-1))$$

The density function contains the information about the synchrony between two states. In case no synchrony is present, the PDF is uniformly distributed and does not exhibit any pronounced peaks. On the other hand, synchronous processes are indicated by distinctive peaks in the PDF (cf. Fig. 1b). This can be analyzed in a quantitative way with the Shannon entropy (Tass et al. 1998):

$$H_{nm}(t;\tau) = -\int_{-\pi}^{\pi} \mathrm{d}\psi\ p_{nm}(\psi, t;\tau)\log(p_{nm}(\psi, t;\tau)) \tag{9}$$

Finally, Eq. (9) is normalized for comparison with the phase coherence. Using a maximal entropy for a uniformly

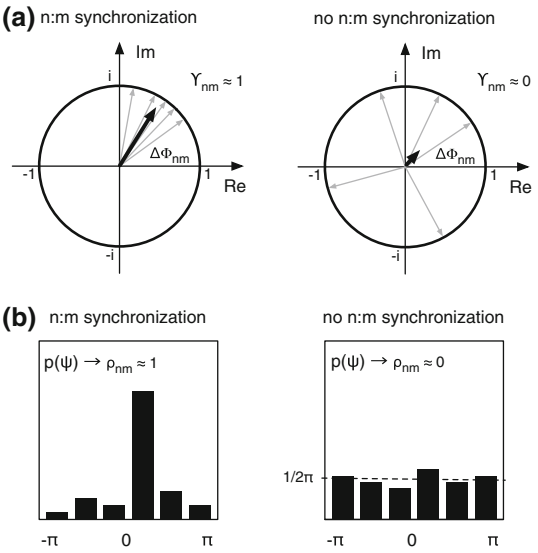


**Fig. 1** Estimation of synchronization is done by (**a**) the average-based $\gamma_{nm}$ and (**b**) a normed entropy-based $\rho_{nm}$. $\gamma_{nm}$ represents the length of averaged unit pointers in the complex plane, whose directions are given by the phase difference. To calculate $\rho_{nm}$ the probability of the cyclic phase differences has to be calculated first. A peaked distribution is an indication for a synchronized state

distributed PDF the result for a normalized synchronization index $\rho_{nm}$ reads:

$$\rho_{nm}(t;\tau) = 1 - \frac{1}{\log 2\pi} H_{nm}(t;\tau) \tag{10}$$

However, in a discrete calculation one has to account for a finite bin size: the factor in Eq. (10) is therefore replaced by $(\ln(N))^{-1}$ (Rosenblum et al. 2001).

We will compare the two measures $\gamma_{nm}(t;\tau)$ and $\rho_{nm}(t;\tau)$ to the standard cross-correlation coefficient $r(t;\tau) \in [-1, 1]$, which is a simple amplitude dependent measure. For this purpose, firstly we write down some abbreviations with the help of a set of stochastic time-series $S^{(j)}(t)$. The tilde denotes the zero-mean time series:

$$\tilde{S}^{(j)}(t) = S^{(j)}(t) - \langle S^{(j)}(t) \rangle \tag{11}$$

and $\sigma\{.\}$ the standard deviation within all trials and the time window $\Delta T$ according to Eq. (5). Applying these abbreviations, we can write down the expression for a time-dependent correlation between two channels $S_k^{(j)}(t)$ and $S_l^{(j)}(t-\tau)$ for a time lag $\tau$:

$$r(t;\tau) = \frac{\langle \tilde{S}_k^{(j)}(t) \tilde{S}_l^{(j)}(t-\tau) \rangle}{\sigma\{S_k^{(j)}(t)\}\ \sigma\{S_l^{(j)}(t-\tau)\}} \tag{12}$$

A number of statistical properties for comparing the quality of synchronization measures are known in the literature (David et al. 2004; Quian Quiroga et al. 2002). For a quantitive comparison of $\gamma_{nm}$, $\rho_{nm}$ and $r$ we measure the distance between the a priori known coupling and the outcome of analysis with a similarity function. As a distance measure we apply the *Jensen–Shannon divergence*, which is a symmetric and bounded version of the *Kullback–Leibler divergence* (Cover and Thomas 1991). The Kullback–Leibler divergence between the known model $\varepsilon(t, \tau)$ and the outcome of our estimated measure $\gamma_{nm}$, $\rho_{nm}$ or $r$, which we abbreviate with $\mu(t, \tau)$, is given by:

$$KL(\mu(t,\tau)||\varepsilon(t,\tau)) = \frac{1}{M^2 - M} \sum_{k \neq l}^{M} \int_0^T \mathrm{d}t \int_0^t \mathrm{d}\tau\, \hat{\mu}_{kl}(t,\tau) \log \frac{\hat{\mu}_{kl}(t,\tau)}{\hat{\varepsilon}_{kl}(t,\tau)} \tag{13}$$

The model $\varepsilon(t, \tau)$ denotes the a priori known connectivity pattern and includes coupling strength between two corresponding sources for the generation of the synthetic data-set, i.e. it depends on the time $t$, the delay $\tau$ and the sources indexed with '$k$' and '$l$', respectively. Equation (13) yields the average of the Kullback–Leibler divergence over all estimated connectivity patterns in a $M \times M$ network without feedbacks within a subsystem $k, l = 1, \ldots, M$. For its estimation one has to consider the normalization of $\mu$ and $\varepsilon$. This is indicated by $\hat{\mu}$ and $\hat{\varepsilon}$ with the property:

$$\int_0^T \mathrm{d}t \int_0^t \mathrm{d}\tau\, \hat{\mu}_{kl}(t,\tau) = 1 \quad \text{and} \quad \int_0^T \mathrm{d}t \int_0^t \mathrm{d}\tau\, \hat{\varepsilon}_{kl}(t,\tau) = 1$$

The Jensen–Shannon divergence can be composed with the use of the Kullback–Leibler divergence in Eq. (13) by

$$JS(\mu||\varepsilon) = \frac{1}{2}(KL(\mu||q) + KL(\varepsilon||q)) \tag{14}$$

and $q = \frac{1}{2}(\mu + \varepsilon)$ denoting the mixture of the model and the data. The distance *JS* offers smoother results than *KL*, whereas in contrast to the *KL* divergence the *JS* will take finite values. The outcome of analysis can be evaluated quantitatively using the Jensen–Shannon divergence Eq. (14) as a similarity function by comparing $\gamma_{nm}(t;\tau)$ Eq. (6), $\rho_{nm}(t;\tau)$ Eq. (10), or $r(t;\tau)$ Eq. (12), with a model $\varepsilon(t, \tau)$.

## Results

### Aperiodically driven stochastic processes

In the first example we want to demonstrate that the detection of synchronization can be applied to non oscillatory fluctuating signals, even if the notion of phase for such wide-band signals is less intuitive than for those that contain a single dominant frequency. This application is important, because first order stochastic dynamical systems can be used for modeling a wide range of complex systems in biology, medicine, physics and engineering (cf. Frank 2004; Haken 2002 2007).

We consider a set of univariate stochastic processes with a directional time delayed linear coupling. We choose the well-described *Ornstein–Uhlenbeck* process, whose dynamics are specified by a deterministic and a stochastic part (Risken and Frank 1996)[1]. For a homogenous Ornstein–Uhlenbeck process the deterministic part is given by a linear damping, $-\alpha X$, resulting in an over-damped movement onto the stable fixed point at $x = 0$. The Langevin force $\Gamma(t)$ drives the system away from its rest position, which results in a random walk like motion relaxing to zero. Adding a term $\xi(t)$ for the coupling force, the '$k$'th process can be written as:

$$\dot{X}_k = -\alpha X_k + \sqrt{Q}\Gamma_k(t) + \xi_k(t) \tag{15}$$

Where $Q$ is the noise amplitude. The Langevin force, $\Gamma(t)$, is an intrinsic white Gaussian dynamical noise, with $\langle \Gamma^{(j)}(t) \rangle_j = 0$. The upper index $(j)$ refers to the $j$th trial of the stochastic process and has been omitted for clarity in Eq. (15). The expression $\langle \cdot \rangle_j$ denotes an average over the

[1] The Ornstein–Uhlenbeck process belongs to the class of Langevin equations. These form an important class of stochastic evolution equations practiced in the field of complex systems (Haken 1977).

trials indexed with '($j$)'. The noise correlation holds $\langle \Gamma_k^{(j)}(t)\Gamma_l^{(j)}(t')\rangle_j = \delta_{kl}\delta(t-t')$, where $\delta_{kl}$ denotes the Kronecker delta, which takes the value one in the case of equal indices $k = l$ for the source indices and zero for unequal index values otherwise. That means $\Gamma(t)$ is an entirely uncorrelated white noise in time and between the processes.

Note that Langevin equations describe continuous but non-differentiable processes, so that strictly the differential quotient d$X$/d$t$ is not well-defined (Gardiner 2009; Risken and Frank 1996). In order to avoid the notation d$X$/d$t$, one may cast Eq. (15) into the form $\mathrm{d}X = -\alpha X\mathrm{d}t + \sqrt{Q}\mathrm{d}W$, where $W$ is a Wiener process with variance proportional to d$t$. For clarity, we use the conventional notation $\dot{X}$ to indicate that these are evolution equations. A stochastic integral can be considered as a limit of the Riemann sum, but the problem arises that the solution of the integral depends on its nodes. In order to interpret the term $\sqrt{Q}\Gamma(t)$ we will use the Itô-interpretation for stochastic integrals (Ito 1944), which applies sinistral nodes in the Riemann sum.

The time-dependent coupling force $\xi_k(t)$ on the '$k$'th source (Eq. 15) includes all time delayed interactions inside the network:

$$\xi_k(t) = \sum_{l\neq k}^{M} \int_0^t \mathrm{d}\tau\, \varepsilon_{kl}(t,\tau)(X_l(t-\tau) - X_k(t)) \qquad (16)$$

In order to include all possible connections in the network we have to sum over the index '$l$' with $l \neq k$ linear coupling terms. We choose a simple linear coupling between the subsystems to exclude unintended complicated nonlinear side effects. We assume no local feedback connections within an oscillator, so $k \neq l$. An integral over the past states $\tau$ is taken to include time delayed influences by the network on the oscillator '$k$'. The upper limit for discovering time delayed synchronization is defined by the current time, which results in the side condition $\tau < t$ regarding that the recording of data starts at $t = 0$. That means if one wants to detect a synchronization to prestimulus activations, prestimulus data has to be recorded. The coupling density $\varepsilon_{kl}(t, \tau)$ contains the complete information of the interconnections of the synthetic network. We chose activation patterns with 2-dim Gaussians in the $(t, \tau)$-plane regarding the constraint $\tau < t$. The time coordinates of all connectivities contained in $\varepsilon_{kl}(t, \tau)$ are summarized in Table 1. The values for the time $t$ and the delay $\tau$ are given in arbitrary units.

The iteration of Eq. (15) was implemented using a Runge–Kutta method of fourth order with a step size of 0.01. We replaced the first step of an explicit Euler step corresponding to the deterministic part of the dynamics with Runge–Kutta steps and consider the stochastic term to be comparable with a Euler-Maruyama method. We chose $\alpha = 10$, $Q = 1$ and the total simulation length $T = 250$ steps. The maximal amplitude of the Gaussian in the coupling $\varepsilon_{kl}(t, \tau)$ was chosen in the range of 4–10 for each connection. As a starting condition the fix point $x^* = 0$ for the homogenous system of Eq. (15) was taken. Furthermore, the first 1000 steps were dismissed. A whole data set was generated by repeating the simulation for $N = 100$ trials.

In Fig. 2a the time series of amplitudes $X^{(j)}(t)$ and the cyclic phase differences $\Psi_{11}^{(j)}(t)$ are plotted for a corresponding pair $j = 1$ with the phase difference and for the remaining $j = 2, \ldots, 100$ trials. One can try to identify the non-delayed coupled states at about $t = 75$ by a closer proximity of two corresponding trajectories $X(t)$ in comparison to uncoupled intervals (cf. the highlighted curves in Fig. 2a). The delayed connectivities cannot be detected just by visual inspection of $X(t)$. The time series of the phase $\Psi_{11}(t;\tau = 0)$ in Fig. 2a show around the coupled regime at $t = 75$ a nearly constant phase, which is disturbed by phase-slips and phase-jumps. In the uncoupled state the phase drifts in a random walk like way.

We now turn to the goal of the detection of phase coupling. The 1st moment of the time series of Eq. (15) vanishes: $\langle X_k^{(j)}\rangle = 0$. In other words, the detection of any connections by estimating averaged activities will not be of help for detecting synchronization. Methods based on simple averaging over the amplitudes would fail for the Ornstein–Uhlenbeck process.

We restrict our analysis on the synchronization order of $n = 1$ and $m = 1$, because the generated data exhibits a

**Table 1** Modeled and recovered locations in the $(t, \tau)$-plane of the Gaussian connectivities $\varepsilon(t, \tau)$

| Source index | | Model $\varepsilon_{kl}(t, \tau)$ | | Recovered $\rho_{11}(t;\tau)$ | |
|---|---|---|---|---|---|
| $k$ | $l$ | $t$ [a.u.] | $\tau$ [a.u.] | $t$ [a.u.] | $\tau$ [a.u.] |
| 2 | 1 | 75 | 0 | 88 | 8 |
| 2 | 1 | 175 | 100 | 190 | 106 |
| 1 | 2 | 125 | 75 | 135 | 83 |
| | | | | See section "Artifacts in bivariate network analysis" | |

Coordinates on the right are given by the center of gravity of the FDR-based clusters of $\rho_{11}$ from the Rössler oscillators (section "Coupled Rössler oscillator"). The index '$k$' denotes the driven and '$l$', the driving index of the 2 × 2 system. The units of the coordinates $t$ and $\tau$ are arbitrary

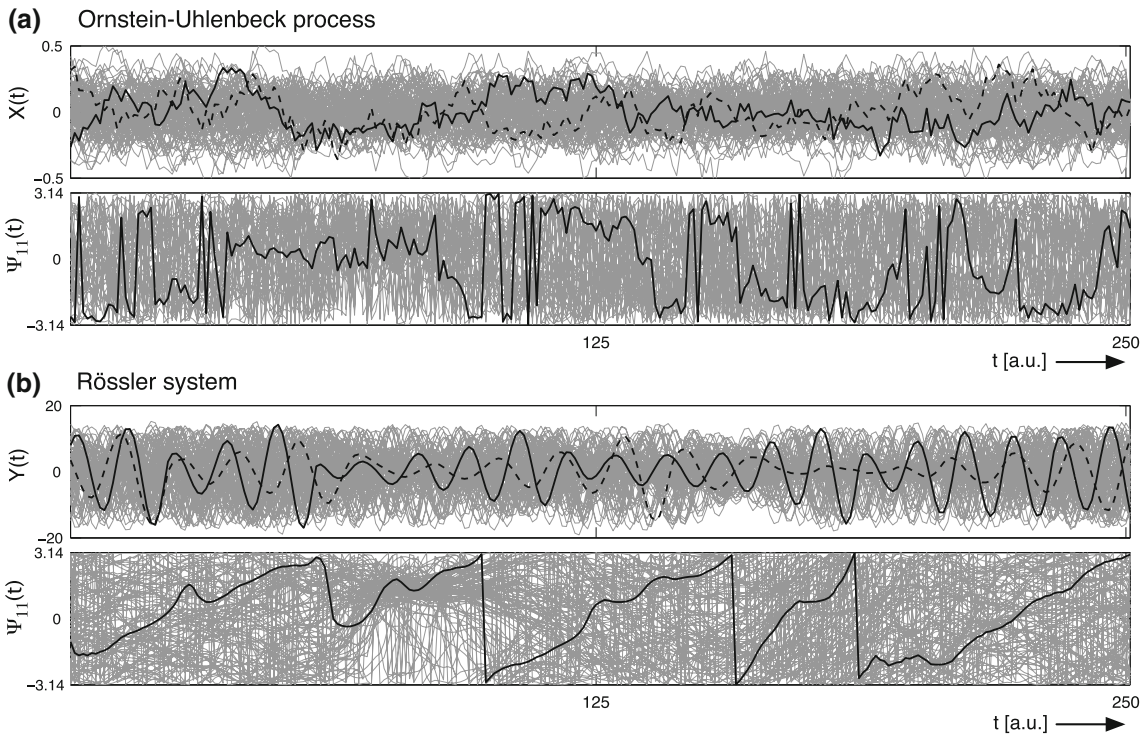


**Fig. 2** 100 simulated trials of the Ornstein–Uhlenbeck (**a**) and the Rössler system (**b**). In (**a**) two corresponding time series of the amplitudes $X(t)$ and cyclic phase differences $\psi_{11}(t)$ for the Ornstein–Uhlenbeck process are plotted in *black*. The *gray colored line* plots show the remaining other trials. In (**b**) the data for the two linked Rössler oscillators are pictured. As amplitude data the y-component $Y(t)$ of each system is taken. Synchronization with $\tau = 0$ occurs around $t = 75$ (cf. Table. 1)

linear coupling term cf. Eq. (16). The linearity results into a direct synchronization of the oscillations, respectively, fluctuations. In Fig. 3a the results of the connectivity analysis for the two mutual coupled Ornstein–Uhlenbeck processes are shown: the absolute value of the correlation coefficient $|r(t;\tau)|$, the phase coherence $\gamma_{11}(t;\tau)$ and the synchronization index $\rho_{11}(t;\tau)$. The subsystems are labeled with the oscillator indices '1' and '2'. One has to consider two possible interconnections for such a system: $k = 1, l = 2$ and $k = 2, l = 1$ with a driving termed '$l$' and the responding system '$k$', which is displayed in each row of Fig. 3. For every connectivity pattern we plot $t$ versus $\tau$ and get results for $\tau < t$, which is given in the region below the diagonal $\tau = t$.

The time axis denotes the time $t$ in view of the responding system, e.g. the connectivity in the plot $k = 1$, $l = 2$ at $t = 125$ and $\tau = 75$ can be understood as an impact of the amplitude of '2' at the retarded time $t' = t - \tau = 50$ on the dynamics of the responder '1' at time $t = 125$, i.e. the plots are displayed in the viewpoint of a responding system. In the first row the a priori known coupling strength $\varepsilon$ for the model input is depicted. The following three rows show the estimates of connectivity achieved with the different methods $|r|$, $\gamma_{11}$ and $\rho_{11}$ for comparison. One can observe directly, that the connections can be identified with all measures, i.e. estimation of the phase works even for raw and unfiltered stochastic data. Compared to the true connectivities (top panels of Fig. 3a) the estimated connectivities are more smeared-out in the $\tau$ direction. This is a property of the simulated data, and not of the synchronization estimates. The effect is a result of the inherent property of a finite friction in every physically motivated system. Driven undamped systems will grow boundless and form therefore no appropriate models. For a Ornstein–Uhlenbeck process the damping is simply given by the parameter $\alpha$. High values of $\alpha$, i.e. a high damping, will result in a fast relaxation onto the fix point, which is in the case of a driven process basically given by the amplitude of the driver $X_l(t - \tau)$. Compared to $\varepsilon_{12}$ at $t = 75$ and $\tau = 0$, one can identify in all estimated measures an erroneous connection. This is a consequence of the symmetry in Eq. (4) for $\tau = 0$. Artifacts are discussed systematically in section "Artifacts in bivariate network analysis".

A comparison of synchronicity measures teach us, that on the one hand the noise background gets more heterogenous from $\rho_{11}(t;\tau)$ over $\gamma_{11}(t;\tau)$ to $|r(t;\tau)|$ (Fig. 4a). On the other hand the signal strength, i.e. the maximal amplitude, decreases from $\max\{|r(t;\tau)|\} \approx 0.72$ over $\max\{\gamma_{11}(t;\tau)\} \approx 0.58$ to $\max\{\rho_{11}(t;\tau)\} \approx 0.12$. The values of $\rho$ are generally lower than $\gamma$ (Rosenblum et al. 2001). Nevertheless, the quality of the $\rho$-patterns is superior due to less fluctuations on larger time scales and more focussed

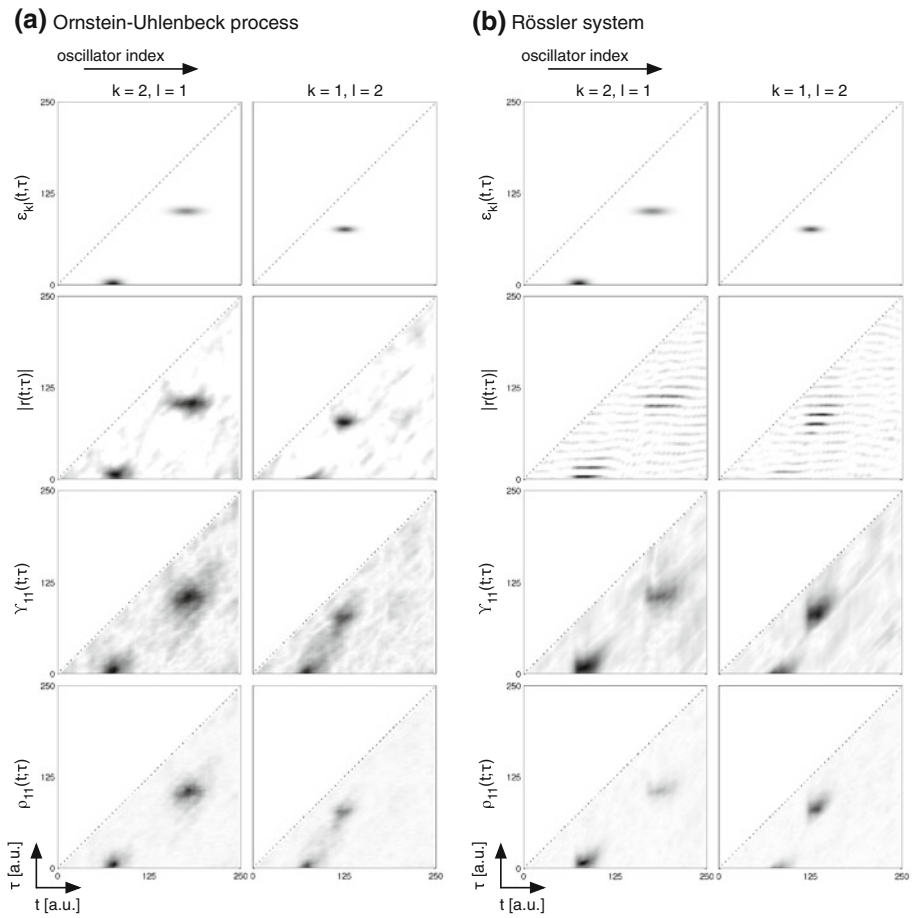


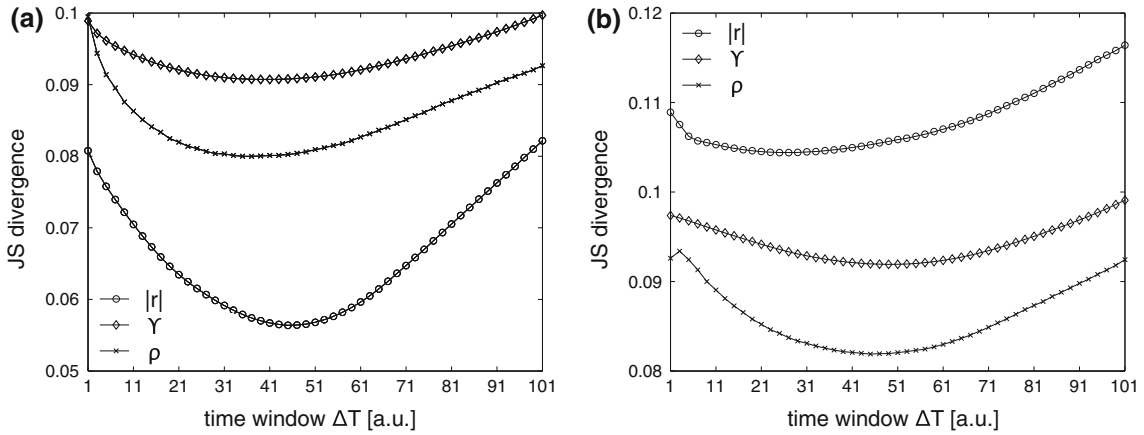


**Fig. 3** Results of the synchronization analysis for (**a**) two Ornstein–Uhlenbeck processes and (**b**) two Rössler oscillators. The scalar field $\varepsilon_{kl}(t, \tau)$ denotes the a priori given coupling density, which is used for the simulation of the data. The window size for the central moving average was chosen with $\Delta T = 9$ time steps for the analysis. The amplitude in the plot for each measure is normalized. *Dark values* indicate high synchronization or correlation respectively

**Fig. 4** The Jensen–Shannon divergence is calculated as a similarity measure between the estimates $|r|$, $\gamma$, $\rho$ and the a priori known coupling strength $\varepsilon$ in dependence of the moving time window sized $\Delta T$ time steps for the Ornstein–Uhlenbeck system (**a**) and the Rössler system (**b**)

peaks of synchronicity compared to the outcome of the phase coherence (Fig. 3a).

The approach of a parametric time-shift $\tau$ allows the detection of connectivities despite small values of synchronization due to the clustering of synchronization in the $(t, \tau)$-plane, i.e. one can distinguish synchronized from unsynchronized regions independently from an absolute threshold. A statistical thresholding of a connectivity pattern is illustrated in the last part of section "Artifacts in bivariate network analysis".

## Coupled Rössler oscillator

In this section we consider non-autonomous stochastic ordinary differential equations of third order, namely modified Rössler oscillators (Rössler 1976). Although the

brain does not generally behave as a chaotic system on a macroscopic scale (Pereda et al. 2005), the Rössler system has the advantage of having periodicity and is therefore complementary to the Ornstein–Uhlenbeck process. For the creation of a dynamical network a number of $M$ of these nonlinear oscillators can be interconnected by a linear delayed coupling as in Eq. (16). With the help of the Rössler oscillator complex oscillatory signals can be generated, whose dynamics underly additionally an inherent noise. After casting the Rössler-equations into a system of differential equations of first order the equation of the '$k$'th oscillator reads:

$$\begin{aligned}\dot{X}_k &= -\omega_k Y_k - Z_k + \sqrt{Q}\Gamma_k(t) + \xi_k(t)\\ \dot{Y}_k &= \omega_k X_k + 0.15 Y_k\\ \dot{Z}_k &= 0.2 + Z_k(X_k - 10)\end{aligned} \tag{17}$$

The cyclic frequency is denoted by $\omega_k$. These are drawn from a Gaussian distribution with a mean $\langle \omega_k^{(j)} \rangle_j = 1$ and the standard deviation of $\sigma_j\{\omega^{(j)}\} = 0.2$ for every trial. Negative frequency values were omitted ($\omega_k^{(j)} > 0$). The intrinsic noise force $\Gamma(t)$ is Gaussian white noise, as in Eq. (15). The noise strength is set to $Q = 1$. For a comparison to the results of section "Aperiodically driven stochastic processes" the same size $M = 2$ and the same positions of the peaks are taken. The maximal amplitudes of the Gaussian coupling density $\varepsilon_{kl}(t, \tau)$ are in the range 0.0016–0.0032. The numerical implementation was done by using a fourth order Runge–Kutta method with a step size of 0.01 and a coarser resampling with $\Delta t = 0.2$, i.e. every 50th step is stored in the data set. As initial condition, a randomized position next to the steady state trajectories is chosen. The first 20 coarse time steps were discarded to reduce transient side effects. Because of a possible applicability to real measurements we chose $N = 100$ trials with 250 data points per trial, as in the section before.

The time series of the y-component are plotted as the amplitude and the phases in Fig. 2b. It is rather difficult to detect the synchronous state just by looking at the data of the oscillatory amplitudes. The phase differences though reveal the synchronous regime of the non-delayed connection. This can be seen due to a higher density of trajectories forming a neck at about $t = 75$ with approximately the same displacement of the phase difference. On the contrary, the collectivity of trajectories outside the synchronous regime are distributed uniformly in the interval $[-\pi, \pi]$. A typical single trajectory within the non-synchronous regime passes in a ramp-like manner, which has its origin in the slow divergence of two corresponding systems (cf. bottom panel of Fig. 2b). The offsets and slopes of these ramps are distributed due to the stochastic properties of the processes (inherent noise, randomized initial values and randomized frequencies) in a random fashion, which results in a uniform density of the entire cohort. The synchronization analysis is also executed for the indices $n = 1$ and $m = 1$. The main difference between the result for the Rössler system and the Ornstein–Uhlenbeck system lies in the correlation $|r(t;\tau)|$: in the analysis of oscillating systems cancellations occurs due to the periodicity of the considered systems (Fig. 3b). Interestingly the phase coherence $\gamma_{11}(t;\tau)$ exhibits exactly the same connectivity pattern, but just without this interference. For the Rössler system the best results with lowest background fluctuations and focussed connectivities provides the synchronization index $\rho_{11}(t;\tau)$ (cf. bottom panel in Fig. 3). As peak values one gets $\max\{|r(t;\tau)|\} \approx 0.86$, $\max\{\gamma_{11}(t;\tau)\} \approx 0.88$ and $\max\{\rho_{11}(t;\tau)\} \approx 0.36$, which indicate strong synchronized states.

A more detailed comparison of the estimated connectivities with the a priori given $\varepsilon$ points out a clearly noticeable difference: connectivities in the model are of Gaussian shape with its symmetry-axis orientated parallel to the $t$- and $\tau$-axis. In the outcome of analysis we find in contrast connectivities forming clusters with borders aligned in parallel to the $\tau$-axis and the $\tau = t$-diagonal. Next, we like to explain this noticeable rhomboid-like shape of the clusters and the partly sharp or smoothed borderlines of the estimated connectivity. A vertical slope on the left border of each cluster can be illustrated if one picks an arbitrary but fixed time point for the receiver. Changing the parameter $\tau$ with a fixed $t$ value results in a movement upwards inside the $(t, \tau)$-plane parallel to the $\tau$-axis. Further, we have to take dynamical effects into account, i.e. we have to consider a synchronization-threshold for complex dynamics as given in a Rössler system (Rosenblum et al. 2001). Therefore, we assume that a sufficiently strong coupling, $\varepsilon(t, \tau) > const$, is exceeded at this time point $t$. If the coupling strength is too small, no synchronization will occur. If the synchronization onset is crossed by passing the synchronization-threshold $\varepsilon(t, \tau) > const$, the synchronized state is reached. This thresholding causes a sharp vertical edge. Once synchronized, a transition to the non-synchronous regime is smoothed out in direction of a further upwards movement to larger $\tau$. This phenomenon can be explained by the self-excited characteristics in the Rössler system: a specific transient time is required for changing its state given by the relaxation time of the system, i.e. that the system responds with a time lag.

An analogous mechanism holds for the contour on the right hand side. It forms a line parallel to the $t = \tau$-line. As an explanation for the different slopes in the $(t, \tau)$-plane compared to the left vertical contour, one has to vary the perspective from the driven to the driving system. For this purpose one visualizes a fixed time point $t' = const$ for the driver. A fixed time in the view of the driving system results in a movement along a line with linear slope of $t = \tau$, because changing the delay time requires a comparable

change of the time $t$ in the responder's view to hold the condition $t' = t - \tau = const$. The sharp-edged transition to the synchronized state can be understood as in the case of the left vertical one by threshold phenomena in synchronizing Rössler oscillators. In comparison to the Rössler system we find for the Ornstein–Uhlenbeck system (Fig. 2a) no sharp-edged transitions on the border of the estimated connectivity clusters. The Ornstein–Uhlenbeck process is not a self-excited system and exhibits not a thresholded transition to the synchronized state. The size of each smeared out connectivity is given by the coupling strength and the damping.

We compared the quality of the analysis outcome with the help of the Jensen–Shannon divergence (Eq. 14). The synchronization-based methods $\gamma$ and $\rho$ behave equally well for the stochastic (Ornstein–Uhlenbeck process) and the chaotic (Rössler system) data (Fig. 4). Overall, $\rho$ performed slightly better in terms of the Jensen–Shannon divergence. The optimal time window $\Delta T \approx 40$ is in the order of the Gaussian window of synchronization in $\varepsilon$ (cf. top panel in Fig. 3). By contrast the amplitude-based $|r|$ performs very differently for the two processes. The reason for this is, that $r$ is very sensitive to periodic behavior. On account of that and because of measurement artifacts on the amplitudes in real MEG data, $r$ is not suited in practice. Remarkably, the phase measures show a comparable quality in the Rössler system and the Ornstein–Uhlenbeck process, despite the problematic of the definition of a phase in stochastic broadband data. This shows that the concept of instantaneous phase is extremely useful in noisy data, such as neuronal signals (EEG, MEG).

## Artifacts in bivariate network analysis

In this section we want to point out some properties of the proposed analysis in principle, namely the occurrence of artifacts and how to deal with them. In our case the term artifact is not to be understood as background fluctuations, but rather as an observable connectivity in form of a cluster in the $(t, \tau)$-plane. Such artifacts can be found in all proposed synchronization measures and are a consequence of the bivariate non-directive character of the approach. Because values in the connectivity pattern can be calculated independently of each other, the artifacts will not affect the overall solution and are therefore a local phenomena in the $(t, \tau)$-plane. We discuss some setups of connectivity patterns, which result in artificial connectivities. One can distinguish three different basic types illustrated in Fig. 5 that might occur in non-directive bivariate analysis: the lack to discriminate the direction in the case of small $\tau \approx 0$ (Fig. 5a), a competition situation with two drivers affecting on a single responder (Fig. 5b) and artifacts generated by an indirect driving (Fig. 5c).

### *Types of coupling and artifacts*

We simulated a network with three Rössler oscillators to illustrate some constructed setups leading to artifacts in the analysis. The same notation is taken for the oscillators as in section "Coupled Rössler oscillator": driving indices are labeled with '$l$' and the responding with '$k$', respectively. In the analysis we account six of the $3 \times 3$ possible interconnections, i.e. the three cases of auto-regulation $k = l$ are omitted. For every oscillator combination one gets a two dimensional connectivity pattern with a time $t$ and a delay $\tau$-axis. All in all the analysis results in a time-dependent $3 \times 3$ symmetrical pattern of connectivity (Fig. 6). Artifacts are marked with a colored dashed circles in the plot for $\varepsilon$ (cf. Fig. 6a). Connectivities causing artifacts are labeled with the corresponding colored letter as used for Fig. 7. The predicted artifacts can be detected in the results shown in Fig. 6b. The interpretation of data especially in larger $M \times M$ networks is laborious. Thus, we want to present a method, which allows a better discrimination of possible artifacts (cf. Fig. 7). Starting with an abstraction of each connectivity cluster to a single $(t, \tau)$-coordinate one is able to reduce extended connectivity patterns to a graph with an improved comprehensibility. In

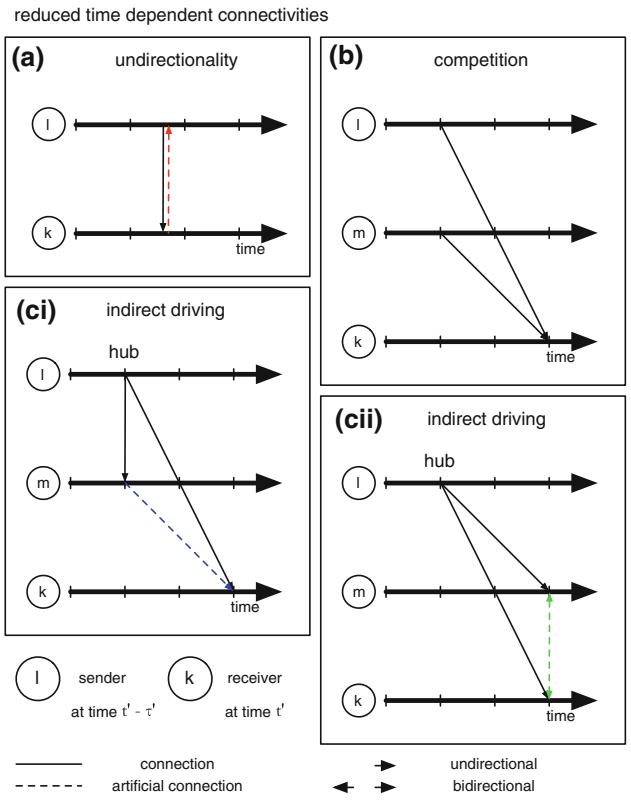


**Fig. 5** A schematic reduction of the time-dependent connectivities $\varepsilon_{kl}(t,\tau)$ to time-dependent graphs is used to explain appearing artifacts in data: (**a**) unidirectionality, (**b**) competition between two driving systems and two special cases of indirect driving (**ci**) and (**cii**)

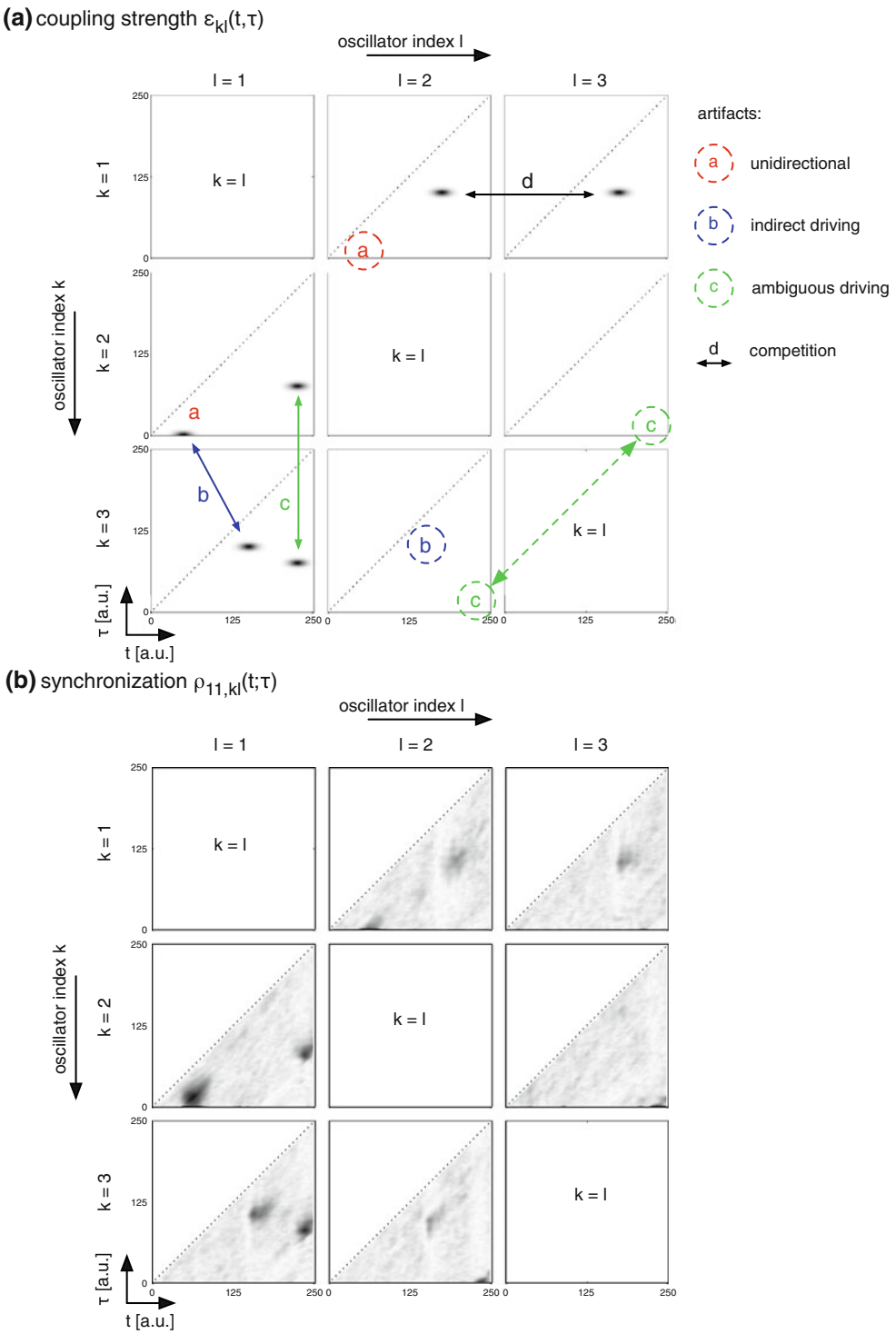


**Fig. 6** Prediction of artifacts in a 3 × 3 network of Rössler oscillators with the a priori known coupling density $\varepsilon_{kl}(t,\tau)$ in (**a**) and the numerical results in (**b**) for the synchronization index $\rho_{11}(t;\tau)$. The *colored labels* in (**a**) are consistent with Fig. 5

the case of a 3 × 3 network the graph consists of 3 lines: a horizontal time line for every subsystem, which is a Rössler oscillator in our example. Each connection or link can be drawn as a directed arrow between two time lines, illustrated as black arrows in Fig. 5. Connections without a time lag are drawn as vertical bidirectional arrows between subsystems as in the example Fig. 5a and ci. A nonzero time delay results in displacement in the horizontal time direction, which actually leads to an unidirectional link between two subsystems. The different types of artifacts are illustrated with the label and colors corresponding to Fig. 7.

In the following part some possible artifacts are discussed for three interconnected oscillators. We constructed

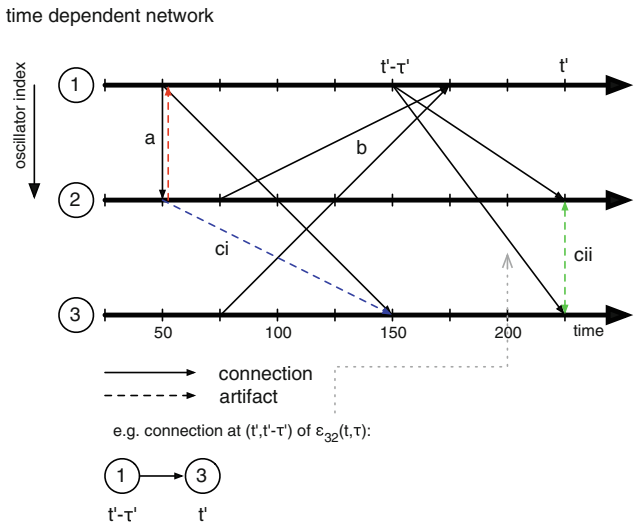


**Fig. 7** Illustration for the connectivities of the reduced patterns $\varepsilon_{kl}(t,\tau)$ shown in Fig. 6. The labels *a–c* correspond to the different cases of Fig. 5

**Table 2** A setup of connectivities to demonstrate some artifacts in the analysis

| Source index | | Model $\varepsilon_{kl}(t, \tau)$ | | Type of artifact |
|---|---|---|---|---|
| $k$ | $l$ | $t$ [a.u.] | $\tau$ [a.u.] | See Fig. 5 |
| 2 | 1 | 50 | 0 | |
| 1 | 2 | 50 | 0 | a |
| 1 | 2 | 175 | 100 | b |
| 1 | 3 | 175 | 100 | b |
| 2 | 1 | 50 | 0 | |
| 3 | 1 | 150 | 100 | |
| 3 | 2 | 150 | 100 | ci |
| 2 | 1 | 225 | 75 | |
| 3 | 1 | 225 | 75 | |
| 3 | 2 | 225 | 0 | cii + a |
| 2 | 2 | 225 | 0 | cii + a |

The artifacts are itemized as in section "Artifacts in bivariate network analysis" with **a** bidirectionality, **b** competition and **ci**, **cii** for the indirect driving

four problematic examples in a 3 × 3 network, which are listed in Table 2.

(a) *Bidirectionality:* First, some artifacts in data are caused by the unidirectionality of the method, i.e. for $\tau = 0$ one is not able to discriminate sender and receiver. In this case connectivity can be detected, but not the causality between two sources. The direction of driving may be separated, if the driver possesses a small delay as in $\varepsilon_{21}$ (Fig. 6). This leads to an asymmetric cluster of the connectivity. The cluster size of the driven system is developed more strongly, i.e. a less pronounced cluster in $k = 1$, $l = 2$.

(b) *Competition:* A further effect is the competition between two driving systems. Strictly speaking, the effect of competition does not generate new artificial connections. In a competitive setup two sources '$l$' and '$m$' have the same receiver '$k$' at the same time (independent of the delayed time of the driver). A competition can reduce the amplitude of synchronization for both drivers, or if the coupling strengths are asymmetrically, the weaker connection may be masked. Such effects depends strongly on the dynamical behavior of the system. In our Rössler system each oscillator exhibits its own cyclic frequency $\omega_k$, and for the case of a frequency mismatch between driver and response the behavior of the driven system depends strongly on the frequency differences and the coupling strength. In a competitive driving an interaction of the driving has to be considered, i.e. synchronous states cannot be superposed simply.

(c) *Indirect driving:* Another class which leads to artificial connectivity is the class of indirect driven processes, i.e. one source '$l$' is a driver of at least two receiver '$m$' and '$k$' at the same time. The problem of measuring the driver-response relationships is addressed by Rosenblum and Pikovsky (2001). In their model they used two mutual coupled phase equations without time lag.

(i) If a source '$m$' is driven with no time lag $\tau' = 0$ and another one '$k$' with a delayed connection $\tau'' > 0$, then '$m$' is an untruly perceived driving of '$k$' with a delay $\tau''$. Additionally, one has to consider a second artificial connection from '$k$' to '$l$' due to the vanishing $\tau'$ as described for the bidirectional case (a).

(ii) As in the first case, a driver '$l$' needs to drive at least two sources '$k$' and '$m$'. Now we consider a same delay time $\tau' = \tau''$. This results in bidirectional connection between '$k$' and '$m$' without a delay.

(iii) In the general case a distributor '$l$' drives at least two sources '$m$' with the delay $\tau' > 0$ and '$k$' with $\tau'' > \tau'$. This can generate an artificial connection from '$m$' to '$k$' with the difference of the delays $\tau = \tau'' - \tau'$.

One can look through these mechanism of indirect driving quite easily, if the connectivity is plotted in a time-dependent graph (Fig. 7). These graphs can be extracted by finding clusters of synchronicity in the $(t, \tau)$-plane. One is able to spot those connections directly, which potentially generate artifacts in synchronicity as discussed before. A driving source with more than one connection to different receivers at the same time can result in an artificial connection between

both receiving systems (cf. Fig. 5ci–ciii). There is still the problem left, that those connections might be no artifacts in real data with a priori unknown connectivity. Moreover, the case of a hidden driver might be problematic, i.e. only the receiving systems are included in the analysis. Both receivers are perceived as connected directly to each other.

These artifacts can be expanded to networks for more than three participant systems and combined to artificial connectivities of higher order. Case (3i) and (3ii) are actually a combination of the general case (3iii) with bidirectional artifacts as in case (1). The important advantage is that results of time-dependent connectivity patterns can be much easier understood, if one illustrates them in the proposed graph than in a full $3 \times 3$ network. In general the Type (a) and (c) artifacts are results of the non-directiveness of the proposed measures of phase synchronization. The effect described as type (b) is a pure dynamical issue and shows a phenomenon, which depends not on the methods itself.

### *Some notes to Granger causality*

With the proposed methods we follow a data-driven approach. The outcome of analysis is independent of parameters or any models. But as a non-directive method the estimated synchronicity is a measure of a correlation (functional connectivity) between two processes and not a direct causality (effective connectivity) between them (Friston 1994). An alternative approach is to measure causality in EEG and MEG data (Kaminski and Blinowska 1991). Granger Causal Modeling (GCM) is based on bi- or multi-variate autoregressive models, which apply roughly spoken a mapping over time lags between two or more time-series (Granger 1969). GCM belongs therefore to the class of model based approaches. It quantifies the information contained in one time series about the outcome of another. In most cases the GCM analysis restricts to linear assumptions for the model. However, there are expansions to nonlinear models (Chen et al. 2004), which requires more data. One can discriminate between the GCM in the time domain (e.g. Seth 2008) and the frequency domain (e.g. Blinowska et al. 2004; Kaminski and Blinowska 1991). The latter is capable of dealing with oscillatory data as generated by a Rössler system. For example Schelter et al. (2006) determined the coherence with a frequency dependent measure based on Granger causality. Usually, GCM assumes a stationary process (but see Ishiguro et al. 2008; Wang et al. 2008). Nolte et al. (2004) discuss the influence of asymmetric noise in GCM, which leads to a bias in the directivity from the channel with less noise to the noisy channel. Due to the symmetry of our proposed method, asymmetric noise in two channels has no effect on the coupling direction.

Especially in the case of neuronal networks the combinatoric possibilities e.g. given just by the total number and location of sources even without considering delayed connections are practically unlimited. For this reason one has to use a hypothesis driven analysis in order to limit the network size to a small number of functional relevant sources. In the approach chosen the results of analysis are independent of a model, i.e. partial solutions of a functional network can simply be superimposed, because no fitting procedure is needed—in particular there is no risk to perform an over-fit of the data. Nevertheless, one can use a hypothesis driven exploration of brain networks with bivariate techniques to reduce a multiplicity of possibilities because a restriction on few sources as a part of a whole functional network will not affect partial solutions.

### *Statistical analysis of the connectivity patterns*

After giving several examples of estimated connectivities from data the question arises, how one can discriminate signal from noise. Finding a proper threshold in multiple comparison can be done by a false discovery rate (FDR) control, which is an established method in fMRI literature (Benjamini and Hochberg 1995; Genovese et al. 2002) and also for coherency patterns in MEG/EEG (Nolte et al. 2004). The idea is to control directly the ratio between false positive voxels and the voxels declared active, which is defined as the false discovery rate. One specifies a parameter $q$ between 0 and 1, which ensures that the FDR is on average not bigger than the chosen rate $q$. The procedure is simple: the $P$-values of a totality of $n = 1, \ldots, V$ values are calculated and then sorted in ascending order.

$$p_n \leq \frac{q}{Vc(V)} \cdot n \tag{18}$$

The parameter q is the tolerated FDR and $c(V)$ is given in general by the expression $c(V) = \sum_{n=1}^{V} 1/n$ (Genovese et al. 2002). The significance threshold is given by the largest $n$, which satisfies the inequality in Eq. (18).

The $P$-values are calculated from a probability distribution of the surrogate data. We use *FT1* surrogates, which are estimated by randomizing the phase in the frequency domain (Palus 1997). The obtained data loses the correlation between its phases without any changes in the frequency spectrum. Next we apply the FDR control on the connectivity pattern of the phase synchronization index estimated from the Rössler system of section "Coupled Rössler oscillator" (Fig. 8). The surrogate pattern is displayed in Fig. 8b. The thresholded image for $q = 0.001$ is shown in Fig. 8c. The coordinates in the pattern are listed in Table 1 and conform with the model data. The thresholded pattern can resolve artifacts regarding the directionality for small delays, i.e. the asymmetry in the

coupling for $k = 2$, $l = 1$ at $t = 75$ is recovered successfully. The bias to larger times and delay times is addressed as a dynamical issue of the friction and was already discussed in section "Coupled Rössler oscillator".

## Discussion

We presented a method for the estimation of time-dependent connectivity patterns applying trial based bivariate analysis of the phases in a network of stochastic oscillators. Phase-based techniques belong to the class of nonlinear methods. We proposed an expansion of phase-based techniques with a parametric delay, which affords no assumptions regarding time delays and temporal dynamics and allows the construction of connectivity matrices. Because the outcome is independent of the included sources within a network, our method can be used to generate models of networks, which can be expanded ad libitum (model-free bivariate analysis). We evaluated the method with two exemplary systems: an Ornstein–Uhlenbeck system, representing a stochastic process, and a Rössler system, representing a chaotic oscillator. Both provide simple models with complex dynamics, a good control over synchronization and are therefore often implemented to test properties of new tools for neuronal synchronization: Quyen et al. (1998) and Quian Quiroga et al. (2002) verified distance measures, Hadjipapas et al. (2005) proved the validity of beamformer mapping the phase correctly and Pereda et al. (2005) discussed the relevance of such systems in the framework of neuroscience.

In our data-model we are not restricted to static coupling terms with a constant delay time. The coupling term of our network given in Eq. (16) is capable of simulating specific time-dependent synchronization patterns with arbitrary time delays. For both systems we demonstrated that the reconstruction of the time-dependent connectivities works even with few data and very diverse system properties such as pure stochastic or oscillatory systems.

We did not test on real data for several pragmatic reasons: The detection of synchronization is a universal phenomenon, which can be applied for a diversity of systems such as oscillatory, chaotic or stochastic ones. Another aspect is that the underlying connectivity pattern is unknown in real data. Moreover, we demonstrated that phase synchronization works with pure broadband stochastic data and we illustrated differences in the results of connectivity comparing stochastic and oscillatory systems.

To quantify the patterns, two different index-based measures of phase synchronization were compared to the correlation coefficient as a more traditional amplitude-based method. The quality was evaluated with the Jensen–Shannon divergence, which allows the estimation of the distance between two distributions—in our case between a given coupling term used for simulating the data and the outcome of the data analysis.

In a third example, we discussed some possible effects and artifacts in networks of three coupled oscillators by means of a 3 × 3 interconnected Rössler system. A driver-response relationship for small delays $\tau \approx 0$ can be revealed by the asymmetry of the connectivity cluster size. This is shown exemplary in section "Artifacts in bivariate network

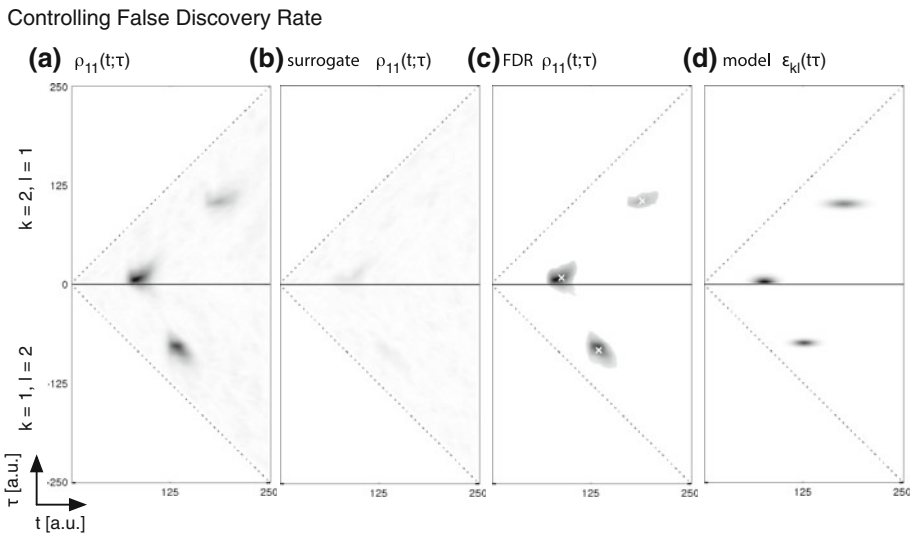


**Fig. 8** The synchronicity within a connectivity pattern can be thresholded by a false discovery rate (*FDR*) control. Two corresponding patterns (for $k = 2$, $l = 1$ and $k = 1$, $l = 2$) are concatenated. (**a**) The phase synchronization index as in Fig. 3 of the Rössler system. (**b**) The synchronization of the surrogate data. (**c**) The image is thresholded by a applying a FDR control with a tolerated false discovery rate of $q = 0.001$. The center of mass for each cluster is indicated by a white cross. The coordinates of the clusters can be found in Table 1. (**d**) The coupling strengths $\varepsilon_{kl}(t, \tau)$ for generating the data

analysis" by calculating the center of gravity for a cluster within the connectivity pattern. The thresholding of the patterns is performed by a FDR control. Then we explored qualitatively the effect of a competition between two driving systems to a single receiver, which results in a decreasing of the synchronicity. Since the magnitude of these effects depends on the dynamics of the system, general statements are difficult. We also were able to predict artificial connections due to the mechanism of indirect driving.

These effects can be predicted conveniently by displaying the results in a time-dependent graph, which we introduced qualitatively (cf. Figs. 5, 7). The extended connectivity patterns can be reduced by links between two sources considering the time delays. The use of abstracted graphs allows a faster interpretation of the time-dependent connections and help to sort out artifacts within the network.

For synchronization with a small delay time the method cannot distinguish the direction of coupling. In that case one can consider the approach of directionality analysis for a classification of driving direction by applying small time increments as delay (Palus et al. 2001; Quian Quiroga et al. 2002; Rosenblum and Pikovsky 2001; Schreiber 2000). They all assumed data in the limit of a non-delayed feedback, respectively coupling term.

Whereas existing methods reveal spatially extended networks (Gross et al. 2004; Lachaux et al. 1999; Stam et al. 2007), the proposed method focusses on trial based data and explore the time dependency of connectivities arbitrary located in the source space.

In comparison to bayesian probabilistic approaches (such as DCM: Friston et al. 2003), the current method requires no internal models. In the work of David et al. (2005) a neural mass model on macroscopic scale was developed, which is capable of simulating event-related responses and is based on the Jansen-Rit model (Jansen and Rit 1995). As a simplified assumption constant delays and a mean-field approximation was taken into account. David et al. (2004) show that several phase-based techniques are able to detect coupling within this framework. Such models are important for a explicit modeling of EEG or MEG signals, which forms the basis on model-based methods like DCM (David et al. 2006; Rudrauf et al. 2008). Another explicit model of electrophysiological data can be implemented by a network of mean-field coupled Fitzhugh-Nagumo neurons (Assisi et al. 2005; Ghosh et al. 2008).

As discussed in section "Artifacts in bivariate network analysis" a popular method of predicting directed connectivity can be performed in terms of the Granger causality by using AR techniques (Granger 1969; Kaminski and Blinowska 1991). In a study of Gow et al. (2008), which combines several multimodal imaging techniques, the non-delayed coherence was used for a preselection of ROIs for a GCM in a second step. The knowledge of specific delays, which could be estimated via connectivity patterns, could be included in a GCM model to reduce the embedding dimension of the autoregression. The expansion of the Granger causality to cyclic variables would be beneficial as presented in the work of Angelini et al. (2009). The problem of a hidden driving could be addressed in a second stage with a multivariate GCM.

We used examples exhibiting linear couplings. For detection of nonlinear interactions, one could expand the method to other information based measure like the index-free mutual information (Kraskov et al. 2004; Palus et al. 2001). David et al. (2004) and Le Van Quyen et al. (2001) show the equivalence of different phase and information measures in electrophysiological data.

**Acknowledgments** M. L. is supported by the German Science Foundation DFG LA-952/3, the German Federal Ministry of Education and Research project Visuo-spatial Cognition, and the EC Projects Drivsco and Eyeshots.

## References

Angelini L, Pellicoro M, and Stramaglia S (2009) Granger causality for circular variables. Phys Lett A 373(29):2467–2470. doi:10.1016/j.physleta.2009.05.009

Assisi CG, Jirsa VK, and Kelso JAS (2005) Synchrony and clustering in heterogeneous networks with global coupling and parameter dispersion. Phys Rev Lett 94(1):018106 doi:10.1103/PhysRevLett.94.018106

Atmanspacher H, Rotter S (2008) Interpreting neurodynamics: concepts and facts. Cogn Neurodyn 2(4):297–318

Barnes GR, Hillebrand A, Fawcett IP, Singh KD (2004) Realistic spatial sampling for MEG beamformer images. Hum Brain Mapp 23:120–127

Benjamini Y, Hochberg Y (1995) Controlling the false discovery rate: a practical and powerful approach to multiple testing. J R Stat Soc Series B Methodol 57(1):289–300

Blinowska KJ, Kus R, Kaminski M (2004) Granger causality and information flow in multivariate processes. Phys Rev E Stat Nonlin Soft Matter Phys 70(5 Pt 1):050902. doi:10.1103/PhysRevE.70.050902

Boccaletti S, Kurths J, Osipov G, Valladares DL, Zhou CS (2002) The synchronization of chaotic systems. Phys Rep 366(1):1–101

Brown R, Kocarew L (2000) A unifying definition of synchronization for dynamical systems. Chaos 10(2). doi:10.1063/1.166500

Chen Y, Rangarajan G, Feng J, Ding M (2004) Analyzing multiple nonlinear time series with extended granger causality. Phys Lett A 324(1):26–35, 2004. doi:10.1016/j.physleta.2004.02.032

Cover TM, Thomas JA (1991) Elements of information theory. Wiley, New York

David O, Cosmelli D, Friston KJ (2004) Evaluation of different measures of functional connectivity using a neural mass model. NeuroImage 21(2):659–673. doi:10.1016/j.neuroimage.2003.10.006

David O, Harrison L, Friston KJ (2005) Modelling event-related responses in the brain. NeuroImage 25(3):756–770. doi:10.1016/j.neuroimage.2004.12.030

David O, Kiebel SJ, Harrison LM, Mattout J, Kilner JM, Friston KJ (2006) Dynamic causal modeling of evoked responses in EEG and MEG Neuroimage 30(4):1255–1272. doi:10.1016/j.neuroimage.2005.10.045

Frank TD (2004) Nonlinear Fokker-Planck equations. Fundamentals and applications Springer Series in Synergetics, 1st edn. Springer, London

Friston KJ (1994) Functional and effective connectivity in neuroimaging: a synthesis. Hum Brain Mapp 2:56–78

Friston KJ, Harrison L, Penny W (2003) Dynamic causal modelling. Neuroimage 19(4):1273–1302. doi:10.1016/S1053-8119(03)00202-7

Gabor D (1946) Theory of communication. J IEEE 93(III)(26):429–457

Gardiner CW (2009) Handbook of stochastic methods: for the natural and social sciences, volume Springer series in syneretics, 4th edn. Springer, London

Genovese CR, Lazar NA, Nichols T (2002) Thresholding of statistical maps in functional neuroimaging using the false discovery rate. NeuroImage 15(4):870–878. doi:10.1006/nimg.2001.1037

Ghosh A, Rho Y, McIntosh A, Kötter R, Jirsa V (2008) Cortical network dynamics with time delays reveals functional connectivity in the resting brain. Cogn Neurodyn 2(2):115–120

Gow DWJ, Segawa JA, Ahlfors SP, Lin F-H (2008) Lexical influences on speech perception: a granger causality analysis of meg and eeg source estimates. NeuroImage 43(3):614–623. doi:10.1016/j.neuroimage.2008.07.027

Granger CWJ (1969) Investigating causal relations by econometric models and cross-spectral methods. Econometrica 37(3):424–438

Gross J, Kujala J, Hämäläinen M, Timmermann L, Schniltzler A, Salmelin R (2001) Dynamic imaging of coherent sources: Studying neural interactions in the human brain. Proc Nat Acad Sci USA 98(2):694–699. doi:10.1073/pnas.98.2.694

Gross J, Schmitz F, Schnitzler I, Kessler K, Shapiro K, Hommel B, Schnitzler A (2004) Modulation of long-range neural synchrony reflects temporal limitations of visual attention in humans. Proc Natl Acad Sci USA 101(35):13050–13055. doi:10.1073/pnas.0404944101

Hadjipapas A, Hillebrand A, Holliday IE, Singh KD, Barnes GR (2005) Assessing interactions of linear and nonlinear neuronal sources using meg beamformers: a proof of concept. Clin Neurophysiol 116(6):1300–1313. doi:10.1016/j.clinph.2005.01.014

Haken H (2002) Brain dynamics: an introduction to models and simulations Springer series in synergetics, 2nd edn. Springer, London

Haken H (2007) Towards a unifying model of neural net activity in the visual cortex. Cogn Neurodyn 1(1):15–25

Haken H (1977) Synergetics: an introduction. Springer, Berlin

Hämäläinen M, Ilmoniemi R (1994) Interpreting magnetic fields of the brain: minimum norm estimates. Med Biol Eng Comput 32(1):35–42

Herdman AT, Wollbrink A, Chau W, Ishii R, Ross B, Pantev C (2003) Determination of activation areas in the human auditory cortex by means of synthetic aperture magnetometry. NeuroImage 20:995–1005 doi:10.1016/S1053-8119(03)00403-8

Hoke M, Lehnertz K, Pantev C, and Lütkenhöner B (1989) Spatiotemporal aspects of synergetic processes in the auditory cortex as revealed by magnetoencephalogram. In: Basar E, Bullock TH (eds) Series in brain dynamics, vol 2. Springer, London, pp 84–105

Ishiguro K, Otsu N, Lungarella M, Kuniyoshi Y (2008) Detecting direction of causal interactions between dynamically coupled signals. Phys Rev E 77(2):026216 doi:10.1103/PhysRevE.77.026216

Ito K (1944) Stochastik integral. Proc Imp Acad Tokyo 20(8):519–524

Jansen B, Rit V (1995) Electroencephalogram and visual evoked potential generation in a mathematical model of coupled cortical columns. Biol Cybern 73(4):357–366

Kaminski M, Blinowska K (1991) A new method of the description of the information flow in the brain structures. Biol Cybern 65(3):203–210

Kraskov A, Stogbauer H, Grassberger P (2004) Estimating mutual information. Phys Rev E Stat Nonlin Soft Matter Phys 69(6 Pt 2):066138 1–16. doi:10.1103/PhysRevE.69.066138

Lachaux JP, Rodriguez E, Martinerie J, Varela FJ (1999) Measuring phase synchrony in brain signals. Hum Brain Mapp 8(4):194–208. doi:10.1002/(SICI)1097-0193(1999)8:4

Le Van Quyen M, Foucher J, Lachaux J, Rodriguez E, Lutz A, Martinerie J, Varela FJ (2001) Comparison of Hilbert transform and wavelet methods for the analysis of neuronal synchrony. J Neurosci Methods 111(2):83–98. doi:10.1016/S0165-0270(01)00372-7

Mormann F, Lehnertz K, David P, Elger C (2000) Mean phase coherence as a measure for phase synchronizationand its application to the EEG of epilepsy patients. Physica D 144(3–4):358–369 doi:10.1016/S0167-2789(00)00087-7

Murakami S, Zhang T, Hirose A, and Okada YC (2002) Physiological origins of evoked magnetic fields and extra-cellular field potentials produced by guinea-pig CA3 hippocampal slices. J Physiol 544(1):327–251 doi:10.1113/jphysiol.2002.027094

Nolte G, Bai O, Wheaton L, Mari Z, Vorbach S, Hallett M (2004) Identifying true brain interaction from eeg data using the imaginary part of coherency. Clin Neurophysiol 115(10):2292–2307. doi:10.1016/j.clinph.2004.04.029

Otnes RK, Enochson L (1972) Digital time series analysis. Wiley, London

Palus M (1997) Detecting phase synchronization in noisy systems. Phys Lett A 235(4):341–351 doi:10.1016/S0375-9601(97)00635-X

Palus M, Komarek V, Hrncir Z, Sterbova K (2001) Synchronization as adjustment of information rates: detection from bivariate time series. Phys Rev E Stat Nonlin Soft Matter Phys 63(4 Pt 2):046211 1–6. doi:10.1103/PhysRevE.63.046211

Pereda E, Quiroga RQ, Bhattacharya J (2005) Nonlinear multivariate analysis of neurophysiological signals. Prog Neurobiol 77(1–2):1–37. doi:10.1016/j.pneurobio.2005.10.003

Pfurtscheller G, da Silva FHL (1999) Event-related EEG/MEG synchronization and desynchronization: basic principles. Clin Neurophysiol 110(11):1842–1857. doi:10.1016/S1388-2457(99)00141-8

Pikovsky A, Kurths J, Rosenblum M (2003) Synchronization: a universal concept in nonlinear sciences, 1st edn. Cambridge University Press, Cambridge

Quian Quiroga R, Kraskov A, Kreuz T, Grassberger P (2002) Performance of different synchronization measures in real data: a case study on electroencephalographic signals. Phys Rev E 65(4):02 (2003)

Quyen MLV, Adam C, Baulac M, Martinerie J, Varela FJ (1998) Nonlinear interdependencies of eeg signals in human intracranially recorded temporal lobe seizures. Brain Res 792(1):24–40. doi:10.1016/S0006-8993(98)00102-4

Risken H, Frank T (1996) The Fokker-Planck equation: methods of solutions and applications, 2nd edn. Lecture Notes in Mathematics. Springer, September 1996

Robinson SE, Vrba J (1998) Functional neuroimaging by synthetic aperture magnetometry SAM In: Biomag 2000, 11th international conference on biomagnetism. Sendai, Japan, pp 1–4

Rosenblum M, Pikovsky A, Kurths J, Schäfer C, Tass PA (2001) Phase synchronization: from theory to data analysis. In: Moss F, Gielen S (eds) Handbook of biological physics, vol 4: neuroinformatics, chap 9. Elsevier, Amsterdam, pp 279–321

Rosenblum MG, Pikovsky AS (2001) Detecting direction of coupling in interacting oscillators. Phys Rev E Stat Nonlin Soft Matter Phys 64(4 Pt 2):045202 1–4. doi:10.1103/PhysRevE.64.045202

Rosenblum MG, Pikovsky AS, Kurths J (1996) Phase synchronization of chaotic oscillators. Phys Rev Lett 76(11):1804–1807.

Rosenblum MG, Pikovsky AS, Kurths J (1997) From phase to lag synchronization in coupled chaotic oscillators. Phys Rev Lett 78(22):4193–4196 doi:10.1103/PhysRevLett.78.4193

Rössler OE (1976) An equation for continuous chaos. Phys Lett A 57(5):397–398 doi:10.1016/0375-9601(76)90101-8

Rudrauf D, David O, Lachaux J-P, Kovach CK, Martinerie J, Renault B, A. Damasio (2008) Rapid interactions between the ventral visual stream and emotion-related structures rely on a two-pathway architecture. J Neurosci 28(11):2793–2803

Rulkov NF, Sushchik MM, Tsimring LS, Abarbanel HD (1995) Generalized synchronization of chaos in directionally coupled chaotic systems. Phys Rev E Stat Phys Plasmas Fluids Relat Interdiscip Topics 51(2):980–994

Schelter B, Winterhalder M, Hellwig B, Guschlbauer B, Lücking CH, Timmer J (2006) Direct or indirect? Graphical models for neural oscillators. J Physiol Paris 99(1):37–46. doi:10.1016/j.jphysparis.2005.06.006 Neuronal Dynamics and Cortical Oscillations

Schreiber T (2000) Measuring information transfer. Phys Rev Lett 85(2):07

Seth A (2008) Causal networks in simulated neural systems. Cogn Neurodyn 2(1):49–64

Stam CJ, Nolte G, Daffertshofer A (2007) Phase lag index: assessment of functional connectivity from multi channel EEG and MEG with diminished bias from common sources. Hum Brain Mapp 28(11):1178–1193. doi:10.1002/hbm.20346

Tass P, Rosenblum MG, Weule J, Kurths J, Pikovsky A, Volkmann J, Schnitzler A, Freund H-J (1998) Detection of n:m phase locking from noisy data: application to magnetoencephalography. Phys Rev Lett 81(15):3291–3294 doi:10.1103/PhysRevLett.81.3291

Toga AW, Mazziotta JC (2002) Brain mapping: the methods, 2nd edn. Academic Press, New York. doi:0-12-693019-8

Van Veen BD, van Drongelen W, Yuchtman M, Suzuki A (1997) Localization of brain electrical activity via linearly constrained minimum variance spatial filtering. IEEE Trans Biomed 44(9):867–880

Varela F, Lachaux JP, Rodriguez E, Martinerie J (2001) The brainweb: phase synchronization and large-scale integration. Nat Rev Neurosci 2(4):229–239. doi:10.1038/35067550

Wang X, Chen Y, Ding M (2008) Estimating granger causality after stimulus onset: a cautionary note. NeuroImage 41(3):767–776. doi:10.1016/j.neuroimage.2008.03.025